



PII: S0749-6419(98)00026-6

## ADIABATIC SHEAR BANDS IN THE TAYLOR IMPACT TEST FOR A WHA ROD

J. B. Stevens and R. C. Batra\*

Department of Engineering Science and Mechanics, Virginia Polytechnic Institute and State University,  
Blacksburg, VA 24061-0219, U.S.A.

(Received in final revised form 20 May 1997)

**Abstract**—We analyse the development of shear bands in axisymmetric, thermomechanical deformations of a circular tungsten heavy alloy (WHA) rod impacting at normal incidence a smooth rigid target. The rod's material is modeled either as a mixture of Fe–Ni–W particles interspread randomly among the W-particles or as a homogeneous alloy. For comparison purposes we also analyse deformations of a pure W and an Fe–Ni–W rod. It is found that shear bands, defined as narrow regions of rapid intense plastic deformation, form near the transition between the mushroomed region and the relatively undeformed portion of the rod, when its material is either a mixture of Fe–Ni–W and W particles or a homogeneous alloy but no such bands form in rods made of either W or Fe–Ni–W only. This could be due to the different initial softening rates of the materials. © 1998 Elsevier Science Ltd. All rights reserved

### I. INTRODUCTION

Dick *et al.* (1991) conducted reverse ballistic impact tests on tungsten heavy alloy (WHA) rods with ellipsoidal tungsten particles in an Fe–Ni matrix and examined the rods for fracture and shear bands. At an impact speed of  $173 \text{ m s}^{-1}$ , the mushroomed end had a slight ellipticity which they attributed to radial cracks in the body. At the higher impact speed of  $228 \text{ m s}^{-1}$ , the deformation was found to be more localized along a curved path extending from the mantle near the transition between the mushroomed region and the relatively undeformed rod toward the impact face. A cusp formed in the lateral boundary where the shear band intersected it. Diametrically opposite to the point where a shear band formed, they observed ductile fracture along a similar path. Some tungsten particles were also deposited on the steel target.

Since Dick *et al.* (1991) gave only the percent composition by weight of the WHA they tested, and no data for the material properties, we simulate their tests by modeling the WHA as a mixture of 10% Fe–Ni–W particles interspread randomly in hard tungsten particles. Three different random distributions are considered, and each material is modeled as isotropic elastic–thermoviscoplastic. The deformations are assumed to be locally adiabatic; thus there is no heat transfer between two contiguous particles. However, the deformations of one affect those of the other since surface tractions and displacements are assumed to be continuous across interelement boundaries. For comparison, we also

---

\*Corresponding author.

model the WHA as a homogeneous, isotropic, thermoviscoplastic material, and analyse deformations of pure tungsten and Fe–Ni–W rods impacting at normal incidence a smooth, flat rigid target.

We note that Taylor (1948) analysed this impact configuration by assuming that when the flow stress is exceeded in the cylinder, a mushroomed region forms near the impacted end. He regarded the mushroomed region as stationary and separate from the undeformed material which continues to move in the direction of impact. Taylor assumed a constant flow stress of the material and related it to the final dimensions of the deformed projectile. Jones *et al.* (1991), (1992) improved upon Taylor's analysis of the problem by dividing it into two phases. The first high strain-rate phase ends with the attenuation of shock waves initiated by the impact. It is followed by a period of lower strain-rate plastic deformations characterized by plastic waves propagating at a uniform speed. These one-dimensional analyses cannot predict details of the deformed configuration of the projectile. Experimental studies (Paparino *et al.*, 1980; Hutchings, 1983) have shown that the Taylor model predicts very approximate values of the dynamic yield strength of the rod's material. Wilkins and Guinan (1973) have shown that the two-dimensional finite difference method provides acceptable predictions of the mushroom profiles; neither of these works focussed on the development of adiabatic shear bands.

## II. FORMULATION OF THE PROBLEM

The thermomechanical deformations of a circular cylindrical rod impacting at normal incidence a smooth, rigid target are governed by the balance of mass, balance of linear momentum, balance of moment of momentum and the balance of internal energy. These balance laws are given in several books, e.g. see Truesdell and Noll (1965). Here we assume the deformations to be locally adiabatic and thus neglect the effect of heat conduction in the balance of internal energy. This assumption is reasonable for the short duration response of the rod, and facilitates evaluation of the temperature field without numerical integration of the energy equation.

The rod is modeled either as a mixture of 10% Fe–Ni–W particles interspread randomly among the tungsten particles with each material taken as isotropic and elastic thermoviscoplastic or as a homogeneous isotropic body made of an elastic thermoviscoplastic material. For each material we hypothesize the following constitutive relations.

$$\boldsymbol{\sigma} = -p\mathbf{1} + \mathbf{S}, p = K(\rho/\rho_0 - 1), \overset{\nabla}{\mathbf{S}} = 2\mu(\overline{\mathbf{D}} - \overline{\mathbf{D}}^p) \quad (1)$$

$$\overset{\nabla}{\mathbf{S}} = \dot{\mathbf{S}} + \mathbf{S}\mathbf{W} - \mathbf{W}\mathbf{S}, \mathbf{D} = \frac{1}{2}(\text{grad}\mathbf{v} + (\text{grad}\mathbf{v})^T), \mathbf{W} = \frac{1}{2}(\text{grad}\mathbf{v} - (\text{grad}\mathbf{v})^T), \quad (2)$$

$$\overline{\mathbf{D}} = \mathbf{D} - \frac{1}{3}(\text{tr}\mathbf{D})\mathbf{1}, \text{tr}\mathbf{D}^p = 0, \mathbf{D}^p = \Lambda\mathbf{S}, S_e^2 \equiv \frac{3}{2}\text{tr}(\mathbf{S}\mathbf{S}^T), \quad (3)$$

$$\sigma_y = (A + B(\dot{\epsilon}^p)^n)(1 + C \ln(\dot{\epsilon}^p/\dot{\epsilon}_0))(1 + \beta - \beta(\theta/\theta_0)^\alpha) \quad (4)$$

$$\dot{\epsilon} = c\dot{\theta} + \text{tr}(\boldsymbol{\sigma}\mathbf{D}^e), (\dot{\epsilon}^p)^2 = \frac{2}{3}\text{tr}(\mathbf{D}^p\mathbf{D}^p). \quad (5)$$

Here  $\sigma$  is the Cauchy stress tensor,  $\mathbf{S}$  its deviatoric part,  $p$  the hydrostatic pressure taken to be positive in compression,  $K$  the bulk modulus,  $\mu$  the shear modulus,  $\overset{\nabla}{\mathbf{S}}$  the Jaumann derivative of  $\mathbf{S}$ ,  $\mathbf{D}$  the deviatoric strain-rate tensor,  $\mathbf{D}^p$  the plastic strain-rate tensor,  $\mathbf{D}^e$  the elastic strain-rate tensor,  $\mathbf{D} = \mathbf{D}^e + \mathbf{D}^p$  the strain-rate tensor,  $\mathbf{W}$  the spin tensor,  $c$  the specific heat,  $\theta$  the temperature of a material particle,  $\theta_m$  its melting temperature,  $\theta_0$  the room temperature,  $S_e$  the effective stress, and  $\epsilon^p$  the effective plastic strain. Equation (1)<sub>2</sub> implies that the volumetric response of the material is elastic. Equation (1)<sub>3</sub> is the constitutive relation in terms of deviatoric stresses for a linear, isotropic hypoelastic material,  $\text{grad } \mathbf{v}$  equals the gradient of the velocity field with respect to co-ordinates in the present configuration, eqn (3)<sub>4</sub> signifies the von Mises yield criterion with isotropic hardening, and eqn (4) is the Johnson and Cook (1983) type relation. Whereas the first two terms in it are the same as those given by Johnson and Cook, the thermal softening term is due to Zhou *et al.* (1994). This softening function describes better the response of the WHA that Zhou *et al.* tested. The flow stress,  $\sigma_y$ , increases with an increase in the effective plastic strain and the effective plastic strain rate but decreases with an increase in the temperature of a material particle. Truesdell and Noll (1965) have pointed out that eqn (1)<sub>3</sub> is not invariant with respect to the choice of different objective (or material frame indifferent) time derivatives of the stress tensor. In eqn (4) parameters  $B$  and  $n$  characterize the strain hardening of the material,  $C$  and  $\epsilon_0$  its strain-rate hardening and  $(1 + \beta - \beta(\theta/\theta_0)^\alpha)$  its thermal softening. Equation (3)<sub>3</sub> signifies that the plastic strain-rate is along the normal to the yield surface described by eqn (3)<sub>4</sub>, and the factor of proportionality  $\Lambda$  is given by

$$\Lambda = 0 \text{ when either } S_e < \sigma_y, \text{ or } S_e = \sigma_y \text{ and } \text{tr}(\overset{\nabla}{\mathbf{S}\mathbf{S}}) < 0; \quad (6)$$

otherwise it is a solution of

$$S_e = (A + B(\epsilon^p)^n) \left( 1 + C \ln \left( \frac{2}{3} \Lambda S_e / \epsilon_0 \right) \right) (1 + \beta - \beta(\theta/\theta_0)^\alpha). \quad (7)$$

Once  $\theta \geq \theta_0(1/\beta + 1)^{1/\alpha}$  at a material point, the flow stress,  $\sigma_y$ , for that material point is set equal to zero. It then behaves like a compressible, nonviscous fluid. In physical experiments, fracture in the form of a crack will ensue from the point well before its flow stress becomes zero. Here we have not incorporated any fracture criterion into the problem formulation. Because a Lagrangian formulation is used and a perfect fluid cannot support shear stresses, once the flow stress at a material point vanishes, the mesh will be distorted quickly and the computations must be stopped. For problems studied herein, the temperature at a material point never became so high as to make the effective stress zero there.

### III. COMPUTATION AND DISCUSSION OF RESULTS

We assigned following values to various material and geometric parameters.

Rod length = 25.4 mm, Rod diameter = 6.35 mm,  $V_0 = 173 \text{ m s}^{-1}$ ,  $\theta_0 = 300 \text{ K}$ .

Tungsten:

$$A = 730 \text{ MPa}, B = 562 \text{ MPa}, C = 0.029, n = 0.0751, \dot{\epsilon}_0 = 1.4 \times 10^{-13} \text{ s}^{-1}, \\ \rho = 19300 \text{ kg m}^{-3}, \mu = 155 \text{ GPa}, K = 317 \text{ GPa}, c = 138 \text{ J kg}^{-1} \text{ }^\circ\text{C}^{-1}, \alpha = 0.15, \beta = 2.4$$

Fe–Ni–W particles:

$$A = 150 \text{ MPa}, B = 546 \text{ MPa}, C = 0.0838, n = 0.208, \dot{\epsilon}_0 = 6.7 \times 10^{-14} \text{ s}^{-1}, \\ \rho = 9200 \text{ kg m}^{-3}, \mu = 98.84 \text{ GPa}, K = 202.4 \text{ GPa}, c = 382 \text{ J kg}^{-1} \text{ }^\circ\text{C}^{-1}, \alpha = 0.2, \beta = 2.4.$$

Tungsten heavy alloy:

$$A = 730 \text{ MPa}, B = 562 \text{ MPa}, C = 0.02878, n = 0.0751, \dot{\epsilon}_0 = 1.355 \times 10^{-13} \text{ s}^{-1}, \\ \rho = 17700 \text{ kg m}^{-3}, \mu = 133.7 \text{ GPa}, K = 273.8 \text{ GPa}, c = 138 \text{ J kg}^{-1} \text{ }^\circ\text{C}^{-1}, \alpha = 0.2, \beta = 2.4.$$

Values of  $A$ ,  $B$ ,  $C$ ,  $n$  and  $\dot{\epsilon}_0$  are derived by curve fitting to those given by Zhou *et al.* (1994). The material subroutine for the Johnson–Cook model in the large scale explicit finite element code DYNA2D (Whirley *et al.*, 1992) was suitably changed to accommodate eqn (4). The DYNA2D code uses 4-noded quadrilateral elements, one-point quadrature rule, and an hour-glass control to suppress the spurious modes. The time step is adjusted adaptively and equals a fraction of the time taken for an elastic wave to travel through the smallest element in the mesh. As elements near the impacted end of the rod are severely deformed, the time step size drops drastically. The initial finite element mesh consisted of uniform square elements of side  $63.5 \mu\text{m}$ . For the rod made of 10% Fe–Ni–W particles and 90% W particles, the material of 10% of the randomly chosen elements was taken to be Fe–Ni–W and of the remaining elements as pure tungsten. The contact condition is satisfied by nullifying the axial velocity of nodes about to penetrate into the target.

Figure 1 depicts for the aforesaid materials the effective stress versus effective plastic strain curves during axisymmetric compression of a homogeneous cylinder deformed at a nominal strain-rate of  $5000 \text{ s}^{-1}$ . The corresponding axial stress versus axial plastic strain curves looked similar to these but exhibited oscillations in the stress. Even though each one of the three materials exhibits softening in the sense that the effective stress decreases with an increase in the effective plastic strain, the initial rate of softening is greatest for the homogeneous WHA alloy. Using perturbation analysis, Wright and Walter (1987) have shown that this initial rate of softening strongly influences the initiation of a shear band. We note that even though values of  $\alpha$  and  $\beta$  in the thermal softening function are same for the Fe–Ni–W particles and the homogeneous WHA alloy, the initial slopes of the softening part of the stress–strain curves are different. This suggests that other material parameters also affect the softening characteristics of a material.

Figure 2(a)–(c) exhibit deformed meshes at  $t = 30 \mu\text{s}$  for three different random distributions of Fe–Ni–W particles. Because of the presence of softer Fe–Ni–W particles, small kinks occurred at several places on the mantle of the rod. However, in each case, only one predominant shear band developed near the point on the rod's mantle where the mushroomed region transitions into the relatively undeformed rod. As observed by Dick

*et al.* (1991) in their experiments, a cusp formed there and the distance of this point from the impact face is nearly the same for the three distributions. The mesh in the nearly 0.2 mm thick dark region adjoining the impact face is also severely deformed. Since the random distribution of Fe–Ni–W particles has a little effect on the development of shear bands in the rod, henceforth we will give results for the random distribution of Fig. 2(b). The deformed mesh at  $t=25\ \mu\text{s}$  for a homogeneous WHA alloy rod shown in Fig. 2(d) reveals deformation patterns similar to those exhibited in Fig. 2(a)–(c). The thickness of the severely deformed region abutting the impact face and the centroidal axis and the peak effective plastic strain are more in Fig. 2(d) than those in Fig. 2(a)–(c). For the homogeneous rod made of either pure tungsten or Fe–Ni–W only, the mantle of the rod was a smooth curve (cf. Figure 2(e) and (f)) and no narrow severely deformed region developed near the point where the mushroomed region transitions into the almost straight mantle. For  $V_0=173\ \text{m s}^{-1}$  the observed deformed lengths and the geometric mean diameter of the impact face were 22.8 mm and  $\sqrt{9.42 \times 9.30}=9.36\ \text{mm}$ , respectively; the corresponding computed values for results plotted in Fig. 2(b), (d)–(f) equalled 22.175, 22.23, 22.119, 21.885 mm and 10.65, 11.25, 10.96, 11.05 mm, respectively. Thus the computed overall dimensions match well with those observed in experiments. The initial speed

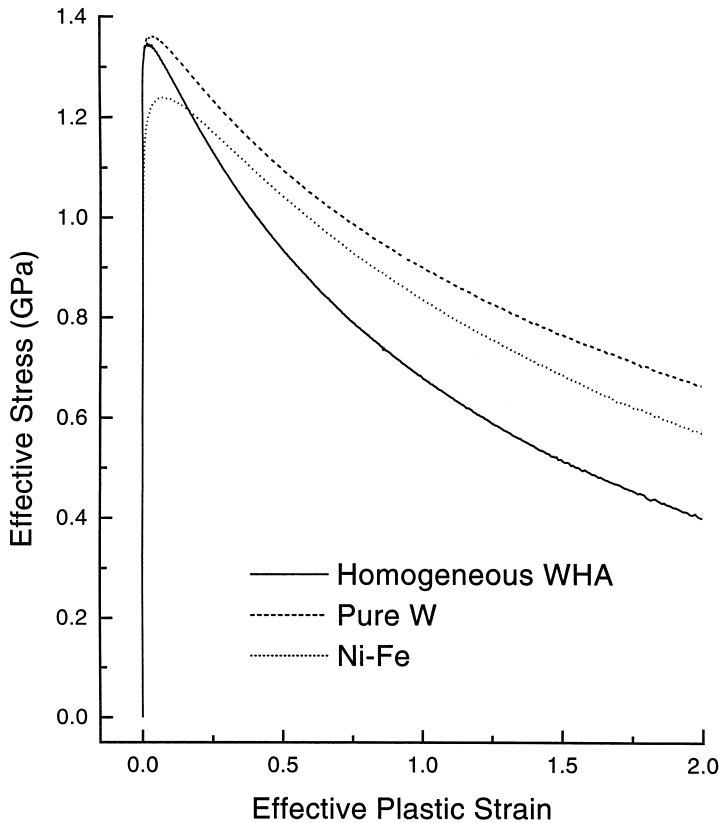


Fig. 1. Effective stress versus effective plastic strain curves for axisymmetric compression at  $5000\ \text{s}^{-1}$  of homogeneous circular cylinders made of (a) WHA, (b) pure tungsten, and (c) Fe–Ni–W particles.

of the Fe–Ni–W rod was  $251 \text{ m s}^{-1}$  so that it had the same kinetic energy as the other rods.

Figure 3(a)–(d) depict fringes of the effective plastic strain in the deformed configurations of the rods corresponding to those shown in Fig. 2(b), (d)–(f), respectively. The fringes in Fig. 3(a) are not smooth because of large variations in the effective plastic strain values in adjoining Fe–Ni–W and pure W particles; the spots signify the Fe–Ni–W particles. Subsequent to impact, the maximum effective plastic strain first occurs, in each rod, at a point near the periphery of the impact face due to the radial expansion of the material there. This point of maximum  $\epsilon^p$  gradually moves towards the rod's axis and becomes

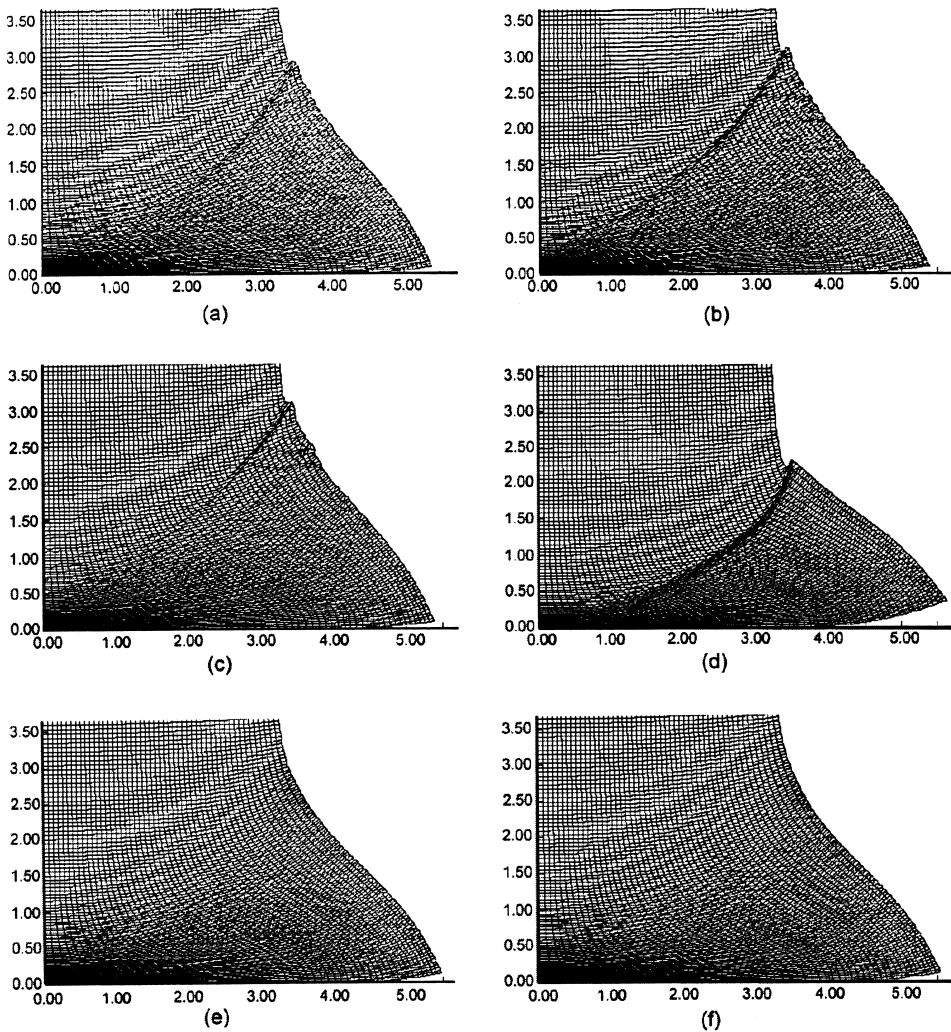


Fig. 2. (a)–(c) Deformed meshes encompassing the mushroomed region at  $t = 30 \mu\text{s}$  for three different random distributions of Fe–Ni–W particles. (d)–(f) Deformed meshes encompassing the mushroomed region when the rod is made of a homogeneous WHA alloy, pure tungsten, and Fe–Ni–W only.

stationary near there. Except when the rod's material is modeled as a homogeneous WHA alloy, the intensely deformed region with the effective plastic strain exceeding 1.0 extends radially on the impact face to nearly 4.5 mm from the centroidal axis; for the WHA rod, it extends radially to only about 3.4 mm. The thickness of this region for the WHA rod is nearly 0.2 mm but equals approximately 0.38, 0.45 and 0.5 mm when the rod's material is modeled as a mixture, pure tungsten and Fe–Ni–W, respectively. A narrow region of intense plastic deformation, extending from the point on the mantle where the mushroomed region transitions into the straight rod to the impact face, has clearly developed in Fig. 3(a) and (b) but not in Fig. 3(c) and (d). This partially explains why the severely deformed disk adjoining the impact face is wider and thicker in Fig. 3(c) and (d) than those in Fig. 3(a) and (b). When the rod is modeled either as a mixture or as a homogeneous WHA alloy, a portion of the kinetic energy of the rod is used up in the development of the shear band. However, for tungsten and Fe–Ni–W rods, the kinetic energy is mainly used to plastically deform the material near the impact face. We have plotted in Fig. 4 the variation of the effective plastic strain on the centroidal axis in the deformed configurations at  $t = 25 \mu\text{s}$  and shown in Fig. 3(a)–(d). For each rod the effective plastic strain drops off rapidly with the distance from the impact face; the effective plastic strain near the stagnation point and the rate of drop of the effective plastic strain with the distance from the impact face is maximum for the homogeneous WHA rod amongst the four materials considered. The oscillations in the curve when the rod is modeled as a mixture are due to the wide variations in the effective plastic strains in Fe–Ni–W and W particles.

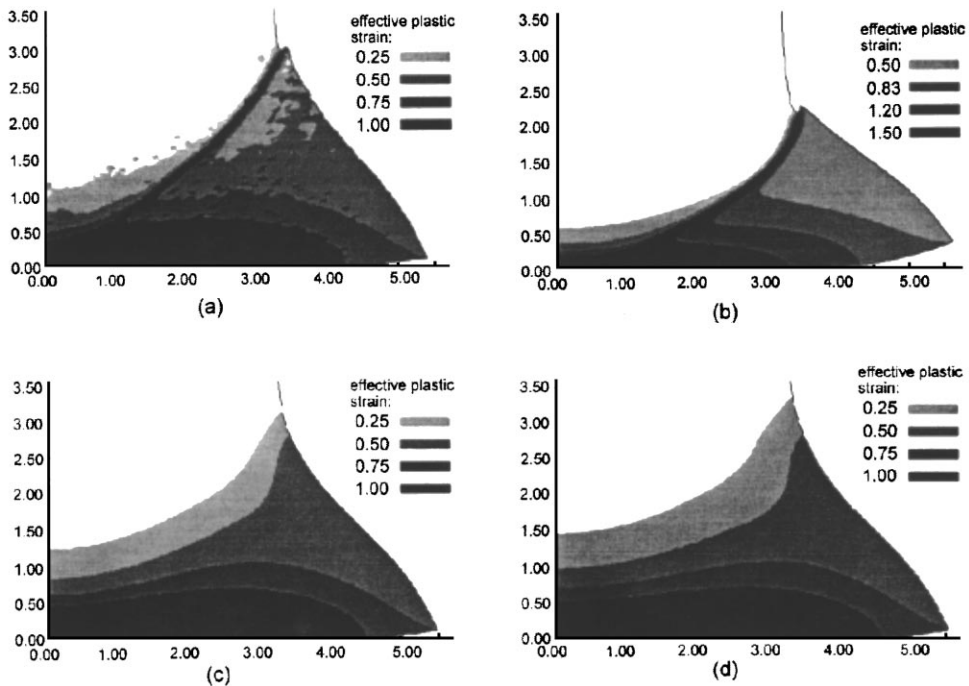


Fig. 3. (a)–(d) Fringes of the effective plastic strain in the deformed configurations corresponding to Fig. 2(b), (d)–(f).

These plots suggest that the thickness of the intensely deformed region near the centroidal axis is at least  $250\ \mu\text{m}$  which far exceeds the usual width,  $20\ \mu\text{m}$ , of a shear band. It is very likely that a material point near the stagnation point,  $r = z = 0$ , will fail first for each rod at a time much before that for which results are plotted in Fig. 3(a)–(d) and a crack will ensue from there. The crack will create new traction free surfaces which may significantly alter the subsequent solution of the problem. However, no such failure criterion has been incorporated in our work.

Results plotted in Figs 2–4 suggest that deformations at the following three locations ought to be examined closely for the initiation of a shear band: point  $P$  adjacent to the stagnation point, point  $Q$  near the periphery of the impacted end, and point  $R$  close to the inflection point in the curve describing the mantle of the deformed rod. For comparison purposes, we also investigate deformations at point  $S$  near the centroidal axis and with about the same distance from the impact face as point  $R$ . In each case, the time histories of the effective plastic strain at these four points are plotted in Fig. 5. For each rod, the effective plastic strain grows very rapidly first at point  $Q$  but the rate of growth drops off and the effective plastic strain there peaks at about 0.8. The effective plastic strain at point  $S$  stays quite low. At point  $P$  near the stagnation point, the effective plastic strain grows

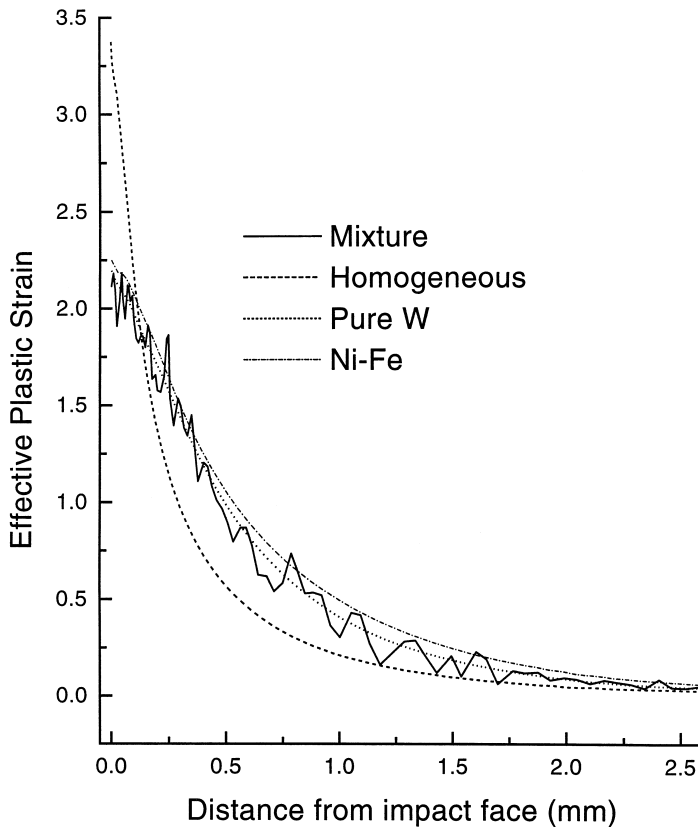


Fig. 4. Distribution of the effective plastic strain on the centroidal axis in the deformed configurations depicted in Fig. 3(a)–(d).

steadily and, for each rod, its maximum value is essentially close to that found in a shear band. However, the thickness of the intensely deformed region near point *P* is much larger than the width of a shear band. Near point *R*, the effective plastic strain continues to grow rapidly when the rod's material is modeled either as a mixture or as a homogeneous alloy but not when the rod is made of either pure W or Fe–Ni–W. As confirmed by the plots of fringes of the effective plastic strain and the deformed meshes, a shear band initiates from point *R* when the material is modeled either as a mixture or as a homogeneous alloy. The width of the shear band can not be delineated because the mesh used, even though finer than that used by others in penetration problems, is relatively coarse and the effects of heat conduction have been neglected. The available computational resources did not allow the use of a finer mesh. The DYN2D code neglects the effects of heat conduction, and it is a nontrivial task to modify it to include heat conduction.

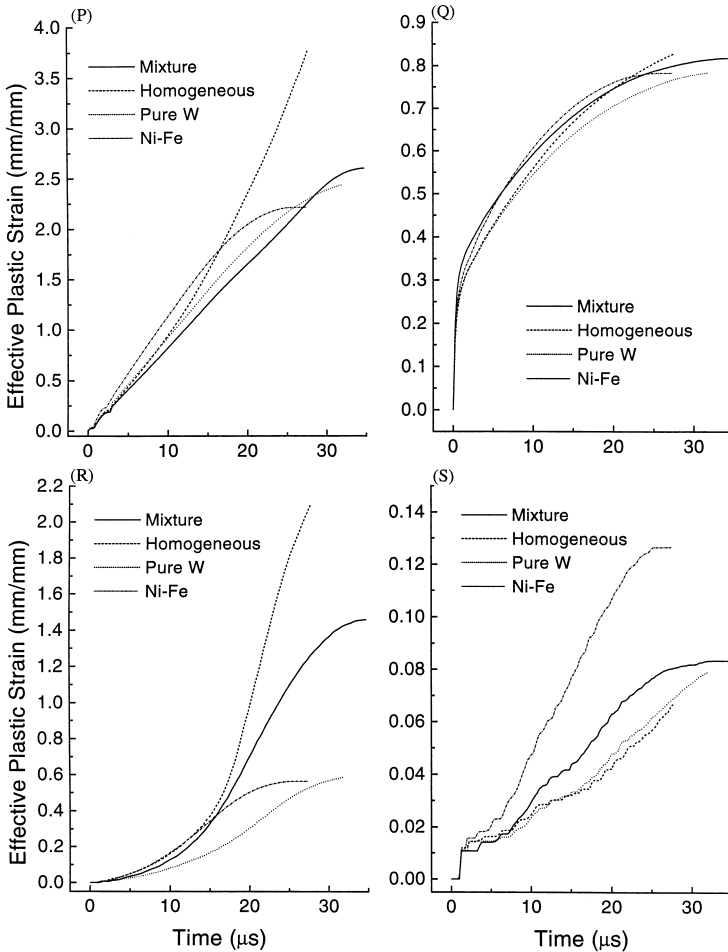


Fig. 5. Time histories of the effective plastic strain at points *P*, *Q*, *R* and *S* for the four material models of the rod.

We have plotted in Fig. 6 the effective stress versus the effective plastic strain for the material particles that in the deformed configurations are at points *P* and *R* when the rod's material is modeled either as a mixture or as a homogeneous alloy. At each point and for both materials, the effective stress drops, the rate of drop of the effective stress is a little higher when the material is modeled as a homogeneous alloy than that for the mixture. Batra and Kim (1992) and Deltort (1994) have postulated that a shear band initiates at a point when the effective stress there drops to 90% and 80%, respectively, of its peak value. According to this definition, a shear band initiates at points *P* and *R* in the

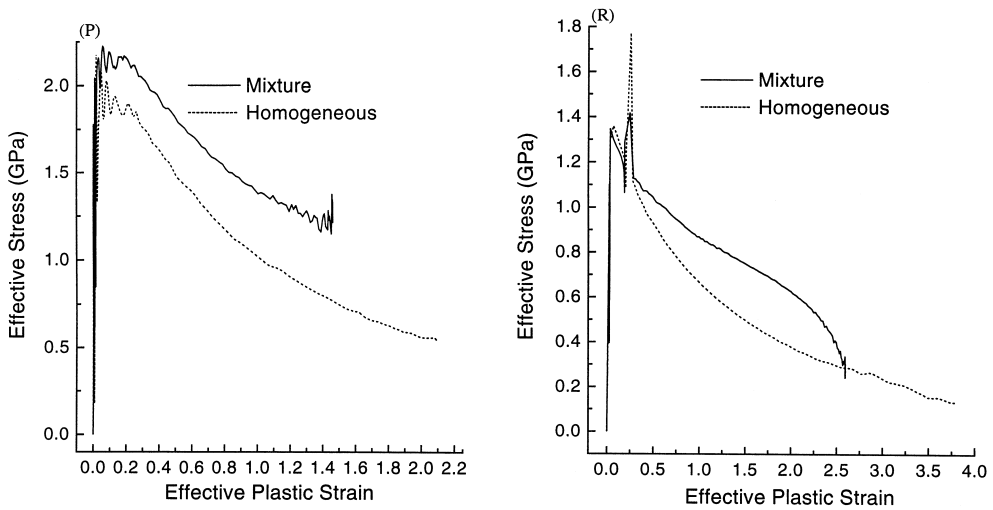


Fig. 6. Effective stress versus effective plastic strain at points *P* and *R* when the rod's material is modeled as a mixture and a homogeneous alloy.

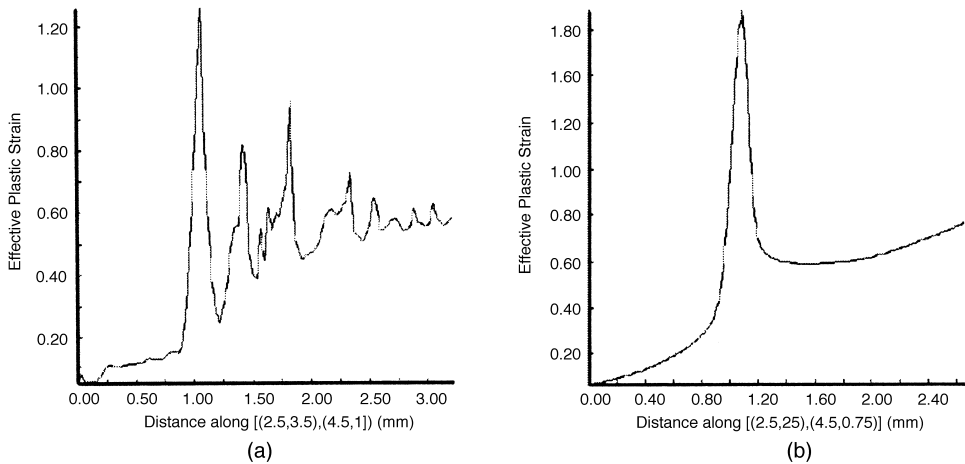


Fig. 7. Distribution of the effective plastic strain on a line nearly perpendicular to the shear band at point *R* when the rod's material is modeled as (a) a homogeneous alloy, and (b) a mixture.

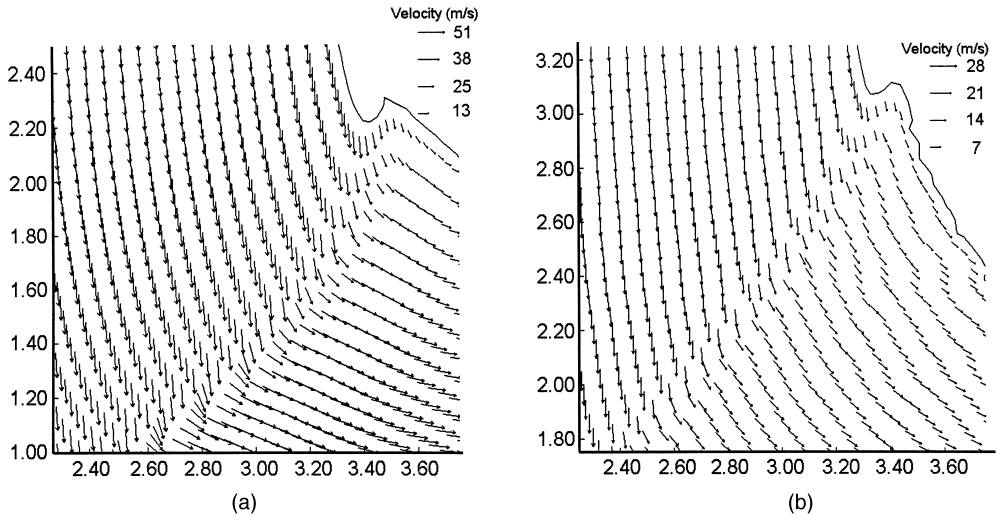


Fig. 8. Velocity field in the region near the cusp in rod's mantle when (a) the rod is modeled as a mixture of Fe-Ni-W particles interspread randomly in *W* particles, and (b) the rod's material is a homogeneous WHA alloy.

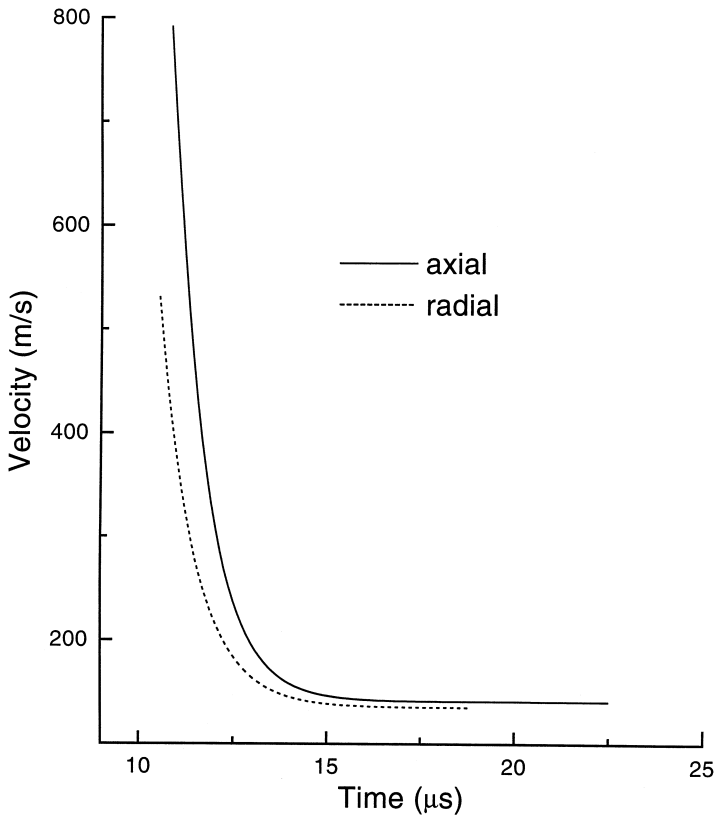


Fig. 9. Speed of propagation, in the reference configuration, of the contour of effective plastic strain of 1.0.

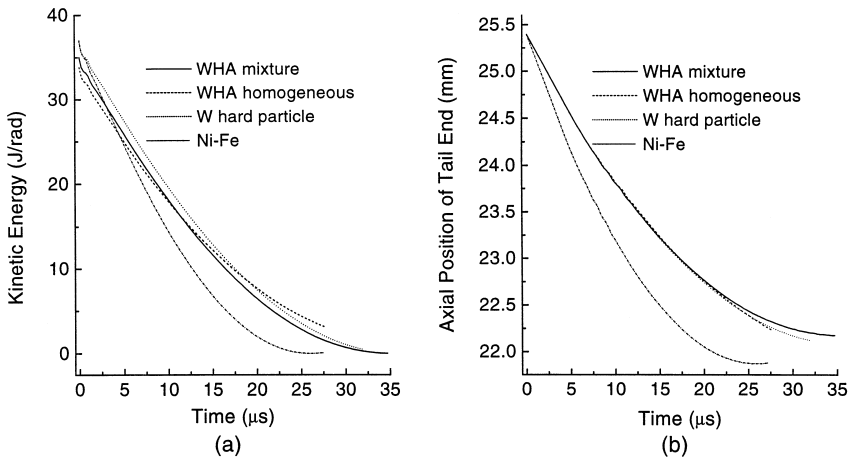


Fig. 10. Time histories of the kinetic energy and the axial position of the tail end of the rod.

homogeneous alloy rod at a lower value of the effective plastic strain than that when the rod's material is modeled as a mixture of Fe–Ni–W and W particles.

For shear bands through point *R* in Fig. 3(a) and (b), we visually determined lines perpendicular to the band. The distribution of the effective plastic strain on these lines, exhibited in Fig. 7, reveals that only one shear band with a peak effective plastic strain of about 1.9 forms when the rod's material is modeled as a homogeneous alloy. However, when the rod's material is modeled as a mixture of W and Fe–Ni–W particles, the peak effective plastic strain in the dominant shear band is 1.3 and there are two additional shear bands with lower values of the peak effective plastic strain. The velocity field in the neighborhood of these bands, plotted in Fig. 8, reveals that the tangential velocity, as conjectured by Tresca (1878), is discontinuous across the band. For plane strain compression of depleted uranium and WHA blocks, Batra and Peng (1995) also found the tangential velocity to be discontinuous across the band.

Needleman (1989), Zhou and Batra (1991) and Batra and Rattazzi (1997) equated the speed of propagation of a shear band to that of a contour of effective plastic strain. Figure 9 illustrates the instantaneous velocities, in the reference configuration, of the contour of effective plastic strain of 1.0 in the axial and radial directions for a homogeneous WHA rod. The speed at the initiation of the contour of  $e^p = 1.0$  from the stagnation point is approximately  $800 \text{ m s}^{-1}$  in the axial direction and  $550 \text{ m s}^{-1}$  in the radial direction. However, this speed drops off rapidly to about  $150 \text{ m s}^{-1}$  in each direction. We note that by plotting the speed of contour of  $e^p = 1.0$  in the reference configuration, we have eliminated the effect of the velocities of material particles. The curves in Fig. 9 are least squares fit to the computed values which oscillated because of errors in estimating the precise time and positions of the contour of  $e^p = 1.0$ .

Figure 10 exhibits the time histories of the kinetic energy of the rod and of the axial position of its tail end. The rate of change of the kinetic energy approximately equals the working of its plastic deformations. The tail end slows down quicker when the rod's material is modeled as a mixture than that for any of the other three material models.

#### IV. CONCLUSIONS

We have analysed axisymmetric, thermomechanical deformations of a WHA rod impacting at normal incidence a smooth rigid target by considering the following four models for the rod's material: Fe–Ni–W particles randomly distributed in W particles, a homogeneous WHA alloy, pure tungsten, and pure Fe–Ni–W. Each material is assumed to be isotropic, and its thermoviscoplastic response represented by the modified Johnson–Cook relation; the modification entails replacing the thermal softening function by that proposed by Zhou *et al.* (1994). In each case, the material in the disk, approximately 4 mm in radius and 0.3 mm thick, adjoining the impact face is intensely deformed.

When the rod's material is modeled either as a mixture of Fe–Ni–W particles inter-spread randomly in W particles or as a homogeneous WHA alloy, a shear band forms at the point on the rod's mantle where the mushroomed region transitions into the straight rod. This agrees qualitatively with Dick *et al.*'s experimental results. However, when the rod is made of either homogeneous tungsten or homogeneous Fe–Ni–W, no such shear band is computed and the mushroomed region transitions smoothly into the relatively undeformed rod. This difference in behaviors could be due to the fact that for the values of material parameters used, the initial rate of softening is highest for the homogeneous alloy. Wright and Walter (1987) have proposed that the initial slope of the thermal softening function strongly influences the initiation of a shear band. For the rod modeled as a mixture of Fe–Ni–W and W particles, the deformations of softer Fe–Ni–W particles may introduce sufficient perturbation to incite localization of deformations at a point on or near the rod's mantle.

*Acknowledgements*—This work was supported by the U.S. Army Research Office grant DAAH04-95-1-0042 to Virginia Polytechnic Institute and State University with Dr K. Iyer as the program manager, and the NSF grant CMS-9411383.

#### REFERENCES

- Batra, R. C. and Kim, C. H. (1992) Analysis of shear bands in twelve materials. *International Journal of Plasticity* **8**, 75–89.
- Batra, R. C. and Peng, Z. (1995) Development of shear bands in dynamic plane strain compression of depleted uranium and tungsten blocks. *International Journal of Impact Engineering* **16**, 375–395.
- Batra, R. C., Rattazzi, D. (1997) Adiabatic shear banding in a thick-walled steel tube. *Computational Mechanics* **20**, 412–426.
- Deltort, B. (1994) Experimental and numerical aspects of adiabatic shear in a 4340 steel. *Journale de Physique, Colloque C8* **4**, 447–452.
- Dick, R. D., Ramachandran, V., Williams, J. D., Armstrong, R. W., Holt, W. H., Mock, W., Jr. (1991) Dynamic deformation of  $W_7Ni_3Fe$  alloy via reverse-ballistic impact. In: Crowson, A., Chen, E. S. (Eds.), *Tungsten and Tungsten Alloys—Recent Advances*. The Minerals, Metals and Materials Society, pp. 269–276.
- Hutchings, I. M. (1983) The behaviour of metals under ballistic impact at sub-ordnance velocities. In: Mescall, J., Weiss, V. (Eds.), *Materials Behavior Under High Stress and Ultrahigh Loading Rates*, 29th Sagamore Army Materials Research Conference. Plenum, New York and London, pp. 161–196.
- Johnson, G. R., Cook, W. H. (1983) A constitutive model and data for metals subjected to large strains, high strain rate, and high temperatures. In: *Proceedings of the 7th International Symposium on Ballistics*, The Hague, The Netherlands, pp. 541–548.
- Jones, S. E., Gillis, P. P., Foster, J. C., Jr. and Wilson, L. L. (1991) A one-dimensional, two-phase flow model for Taylor impact specimens. *Journal of Engineering Materials and Technology* **113**, 228.
- Jones, S. W., Maudlin, P. J., Gillis, P. P., Foster, J. C. Jr. (1992) Material behavior during early time plastic deformation in the Taylor impact test. In: *Computers in Engineering*, vol. 2. ASME Press, New York, pp. 173–179.
- Needleman, A. (1989) Dynamic shear band development in plane strain. *Journal of Applied Mechanics* **56**, 1–8.
- Papirno, R. P., Mescall, J. F., Hansen, A. M. (1980) Beyond the Taylor test to fracture. In: *Proceedings of the Army Symposium on Solid Mechanics, 1980—Designing for Extreme Environments, Loading and Structural Behaviour*. Army Materials and Mechanics Research Center, Watertown, MA, pp. 367–385.

- Taylor, G. I. (1948) The use of flat-ended projectiles for determining dynamic yield stress I. Theoretical considerations. *Proceedings of the Royal Society* **A194**, 289–299.
- Tresca, H. (1978) On further application of the flow of solids. *Proceedings of the Institute of Mechanical Engineers* **30**, 301.
- Truesdell, C. A., Noll, W. (1965) The nonlinear field theories of mechanics. In: Flügge, S. (Ed.), *Handbuch der Physik*, vol. III/3. Springer-Verlag, Berlin.
- Whirley, R. G., Engelmann, B. E., Hallquist, J. O. (1992) DYN2D, A Nonlinear, Explicit, Two-Dimensional Finite Element Code for Solid Mechanics, User Manual, Lawrence Livermore National Laboratory Report, UCRL-MA-110630.
- Wilkins, M. L. and Guinan, M. W. (1973) Impact of cylinders on a rigid boundary. *Journal of Applied Physics* **44**, 1200.
- Wright, T. W. and Walter, J. W. (1987) On stress collapse in adiabatic shear bands. *Journal of the Mechanics and Physics of Solids* **35**, 701–720.
- Zhou, Z. G. and Batra, R. C. (1991) Shear band development in a thermally softening viscoplastic body. *Computers and Structures* **39**, 459–472.
- Zhou, M., Needleman, A. and Clifton, R. J. (1994) Finite element simulations of plate impact. *Journal of the Mechanics and Physics of Solids* **42**, 423–458.